JOURNAL OF SPACECRAFT AND ROCKETS
Vol. 36, No. 1, January–February 1999

Fabrication and Testing of Mo–Re Heat Pipes Embedded in Carbon/Carbon

David E. Glass*
Analytical Services and Materials, Inc., Hampton, Virginia 23666
Charles J. Camarda†
NASA Johnson Space Center, Houston, Texas 77058
and
Michael A. Merrigan‡ and J. Tom Sena§
Los Alamos National Laboratory, Los Alamos, New Mexico 87545

Two heat-pipe test articles were fabricated and tested, furthering the development of a refractory-composite/heat-pipe-cooled leading edge. A 3-ft-long, molybdenum–rhenium heat pipe with lithium working fluid was fabricated and tested in a vacuum chamber at an operating temperature of 2460°F, verifying the heat-pipe design. Following the fabrication of the initial heat pipe, three additional heat pipes were fabricated and embedded in carbon/carbon. The carbon/carbon heat-pipe test article was successfully tested using quartz lamps in a vacuum chamber in both horizontal and vertical orientations. Startup and steady-state data indicated similar operation in both orientations but different behavior among the three heat pipes. Radiography and eddy current evaluations were performed on the test article and indicated differing carbon/carbon thicknesses and a potential disbond.

Nomenclature

d = artery diameter, in.
m = mass of lithium in heat pipe, lb
P = pressure, psi
q = heat flux, Btu/s
q'' = heat flux per area, Btu/ft^2-s
r = radius, in.
T = temperature, °F
t = time, s
V = voltage, V
x = distance from end of carbon/carbon, in.

Introduction

STAGNATION regions, such as wing and tail leading edges and nose caps, are critical design areas for hypersonic aerospace vehicles because of the hostile thermal environment those regions experience during flight. As a hypersonic vehicle travels through the Earth's atmosphere, the high local heating and aerodynamic forces cause extremely high temperatures, severe thermal gradients, and high stresses. Analytical studies and laboratory and wind-tunnel tests indicate that a solution to the thermal-structural problems associated with stagnation regions of hypersonic aerospace vehicles might be alleviated by the use of heat pipes to cool these regions.[1–12] Recent work to develop a novel refractory-composite/refractory-metal heat-pipe-cooled leading-edge concept for hypersonic vehicles combines advanced high-temperature materials, coatings, and fabrication techniques with an innovative thermal-structural design. Preliminary design studies indicate that a heat-pipe-cooled leading edge can reduce the leading-edge mass significantly compared to an actively cooled leading edge, can completely eliminate the need for active cooling, and has the potential to provide failsafe and redundant features.[13] Studies have also been performed on the use of carbon/carbon (C/C) heat pipes for space nuclear power applications by Rovang et al.[14] evaluating C/C tubes with metallic liners for use as heat pipes.

The present paper discusses several tests to help verify the fabrication and performance of a heat-pipe-cooled leading edge for hypersonic vehicles (also see Ref. 15). A 3-ft-long molybdenum–rhenium (Mo–Re) D-shaped heat pipe was fabricated and heated with induction heating in a vacuum chamber to an operational temperature of 2460°F. The heat pipe used lithium as the working fluid and had a D-shaped cross section. The same design was used to construct three additional heat pipes, which were embedded in C/C. The C/C test article was tested with quartz lamps in a vacuum chamber in both vertical and horizontal orientations.

Description of Heat-Pipe-Cooled Leading-Edge Concept

A brief description of how heat pipes operate and are utilized for leading-edge cooling is first presented, followed by a description of the proposed heat-pipe-cooled leading-edge concept.

Leading-Edge Heat-Pipe Operation

Heat pipes transfer heat nearly isothermally by the evaporation and condensation of a working fluid. The heat is absorbed within the heat pipe by evaporation of the working fluid. The evaporation results in an internal pressure differential that causes the vapor to flow from the evaporator region to the condenser region, where it condenses and gives up heat. The cycle is completed with the return flow of the liquid condensate to the evaporator region by the capillary action of a wick.

Heat pipes provide cooling of leading-edge stagnation regions by transferring heat nearly isothermally to locations aft of the stagnation region, thus raising the temperature aft of the stagnation region above the expected radiation equilibrium temperature. When applied to leading-edge cooling, heat pipes operate by accepting heat at a high rate over a small area near the stagnation region and radiating it at a lower rate over a larger surface area, as shown in Fig. 1. The use of heat pipes results in a nearly isothermal leading-edge surface, reducing the temperatures in the stagnation region and raising the temperatures of both the upper and lower aft surfaces.

Received March 10, 1998; revision received June 24, 1998; accepted for publication Aug. 26, 1998.

*Senior Scientist, 107 Research Drive. Senior Member AIAA.
†Astronaut, Astronaut Office, Mail Code CB, 2101 NASA Road 1. Associate Fellow AIAA.
‡Deputy Group Leader, Energy and Process Engineering, Retired; currently Technical Staff Member, Comforce, Inc., Los Alamos, NM 87545.
§Staff Member, Energy and Process Engineering, P.O. Box 1663, Mail Stop J576.

C/C Heat-Pipe-Cooled Wing Leading Edge

A C/C heat-pipe-cooled wing-leading-edge concept is shown in Fig. 2 (Ref. 16). The heat pipes are oriented normal to the leading edge and have a D-shaped cross section, with the flat part of the D forming the wing-leading-edge outer surface. A cross section of the leading edge (Fig. 2) shows the D-shaped heat pipes embedded in the C/C. An alternating J-tube configuration was selected to minimize heat-pipe spacing in the nose region, where heating is highest, and at the same time minimize mass. The C/C structure sustains most of the mechanical structural loads and also offers ablative protection in the event of a heat-pipe failure.

The maximum operating temperature capability of coated C/C composite materials for the primary structure of the leading edge is high (~3000°F) relative to refractory metals, which are typically limited to approximately 2400°F. The potentially higher operating temperature of the present concept increases the radiation heat-rejection efficiency of the heat-pipe-cooled leading edge and permits reductions in the mass of the leading edge for a given leading-edge radius. In addition, the higher operating temperature increases the total heat load that can be accommodated passively by the heat pipe, i.e., no forced convective cooling required. For many trajectories, the high operating temperatures of the present design help eliminate the need for active cooling during both ascent and descent, thus eliminating the need for carrying additional hydrogen fuel (coolant) into orbit. Because many hypersonic vehicles return unpowered for landing, the additional hydrogen fuel needed for cooling during descent would result in a mass penalty.

Results and Discussion

Initially, a single heat pipe with a D-shaped cross section was fabricated and tested to 2460°F in a vacuum. Upon determining that the heat-pipe design was adequate, three additional heat pipes were fabricated. These three heat pipes were then embedded in C/C and tested in a vacuum chamber. A discussion of each of these heat-pipe tests follows.

Design Validation Heat Pipe

A D-shaped heat pipe was fabricated and tested to determine the performance characteristics of the heat pipe designed for cooling the wing leading edge. A description of the fabrication procedure for the heat pipe is given, followed by a discussion of the heat-pipe testing. Both the fabrication and testing of the design validation heat pipe were performed at Los Alamos National Laboratory (LANL).

The artery was fabricated by wrapping three layers of 400 × 400 mesh Mo–5Re screen around a 0.125-in.-outer-diameter steel mandrel, which was held in place with a 0.003-in.-diam steel wire spirally wrapped the length of the artery. The steel mandrel/screen assembly was inserted into a 0.25-in.-outer-diameter × 0.035-in. wall steel sheath. The steel sheath was drawn down to a 0.210-in. outer diameter. After the final draw, the assembly was immersed in a water/hydrochloric solution, and the steel mandrel, sheath, and wire were dissolved leaving the formed screen artery.

The screen wick was fabricated by wrapping the first two layers of 400 × 400 mesh screen over a copper mandrel that had been machined to the wick's final shape. The artery was placed over the first two layers of screen, the final two layers of screen were wrapped over the mandrel, and the artery and the edge of the final wrap was spot welded the length of the wick. The assembly was then slid off the copper mandrel.

The heat pipe was fabricated from a Mo–41Re D-shaped tube that was drawn from an arc-cast bar at Thermo Electron Tecomet, Wilmington, Massachusetts. A screen wick was fabricated by wrapping four layers of 400 × 400 mesh Mo–5Re screen around a D-shaped mandrel. Figure 3 shows a photograph of a section of the D tube and the screen wick. The artery is located in the top center of the curved portion of the heat pipe and has a spring in it to help maintain its shape. Superimposed in Fig. 3 is a photograph of the closeout at one end of the wick. One end of the wick is closed out as in the photograph, and the other end is open and is covered by a pool of liquid lithium during operation. Mo–41Re end caps were machined and welded to the ends of the heat pipe.

After the heat pipe was assembled, Li vapor was distilled into the heat pipe. A schematic diagram of the distillation apparatus and a detailed description of the distillation process are given in Ref. 17. The distillation pot was heated by induction heating. All of the lithium was distilled into the heat pipe to ensure the purity of the lithium. After the lithium was distilled into the heat pipe, the heat pipe was closed by the use of a valve.

The heat pipe was then instrumented with thermocouples. One thermocouple was located over the evaporator section end cap, whereas the remaining thermocouples were spaced along the condenser as shown schematically in Fig. 4. A thin piece of $\frac{1}{16} \times \frac{1}{4}$ in. Ni foil was spot welded to the Mo–Re heat pipe. W/W-26Re thermocouples were then spot welded to the Ni foil. The accuracy of

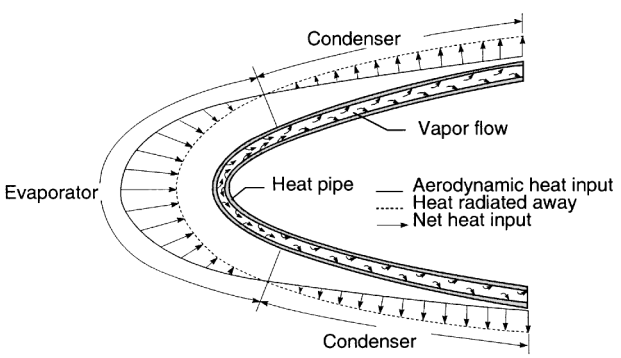

Fig. 1 Schematic diagram of a heat-pipe-cooled leading edge showing regions of net heat input (evaporator) and net heat output (condenser).

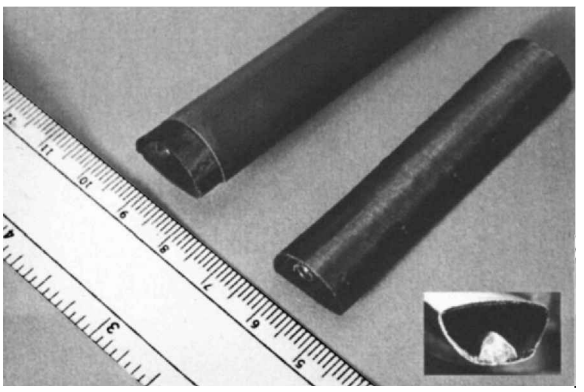

Fig. 3 Photograph of a section of D tube and screen wick.

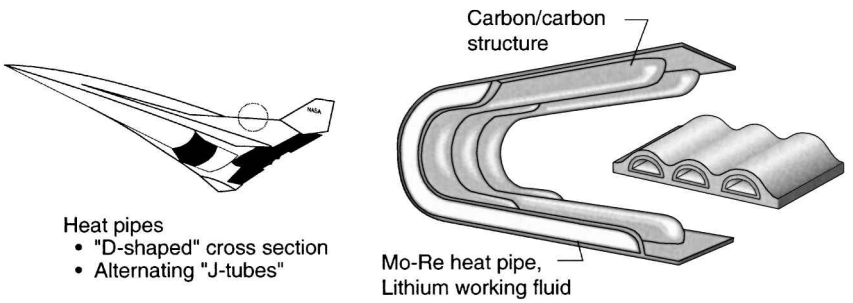

Fig. 2 Schematic drawing of a hypersonic vehicle with a diagram of a heat-pipe-cooled wing leading edge.

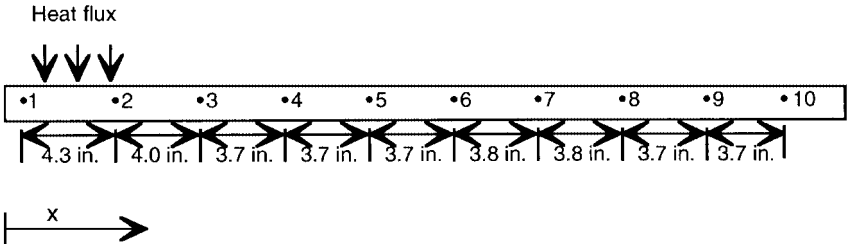

Fig. 4 Schematic diagram showing the location of the thermocouples on the heat pipe.

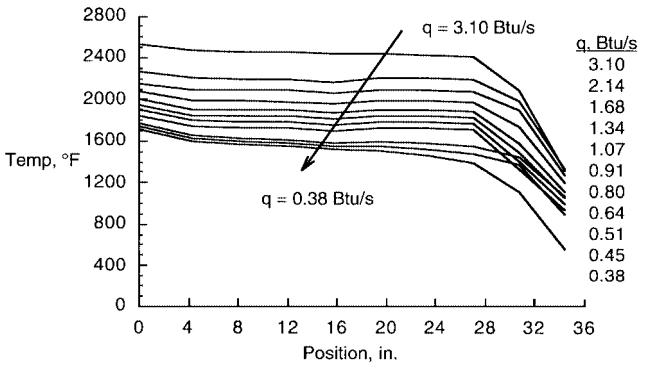

Fig. 5 Steady-state temperature distributions for a range of heat fluxes, $T = \pm 1\%$.

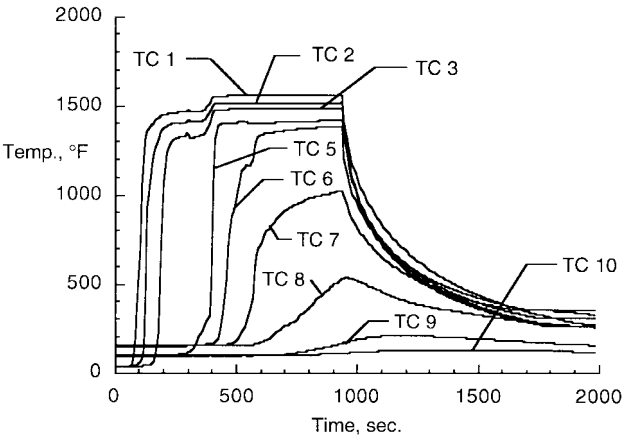

Fig. 6 Temperature vs time at various thermocouple locations during startup from the frozen state of a Li/Mo–Re heat pipe, $T = \pm 1\%$ above 800°F.

the thermocouples is ±8°F below 800°F and ±1% above 800°F. All of the thermocouples were centered on the flat portion of the heat pipe.

The D-shaped Mo–Re heat pipe was placed in a vacuum chamber and heated by induction heating. The induction heating coils initially covered approximately 4 in. of the heat-pipe length. After several preliminary tests in which the D-shaped Mo–Re heat pipe was checked to ensure proper operation, the steady-state throughput of the heat pipe was measured at different power supply settings. The throughput was the total integrated heat flux into the evaporator that was transferred to the condenser and radiated away by the outer surface of the heat pipe. Prior to calibration, the length of the induction heating coils was reduced from 4 to 2 in. This reduction enabled the heat flux to be doubled while maintaining the same throughput and maximum operating temperature.

During calibration, the heat pipe was slowly brought to a temperature of 2370°F, and steady-state operation was obtained at various intermediate temperatures, as shown in Fig. 5. As can be seen, the temperatures are relatively uniform except at the two ends of the heat pipe. The first thermocouple in the evaporator end was over the end cap and was not cooled by the lithium, thus resulting in slightly higher temperatures. At the condenser end, a lithium pool resulted in cooler thermocouple temperatures. The temperatures were monitored with both an optical pyrometer and thermocouples spot welded on the heat pipe. Knowing the steady-state temperature of the heat pipe, the heat radiated away (the throughput) could be related to the setting on the power supply. The throughputs for the steady-state conditions are listed in Fig. 5. However, because of the temperature dependence of the electrical resistance of the Mo–Re, the heat input at a given power setting is different for different heat-pipe temperatures. Thus, the heat input determined from the measured throughput is not as accurate during transient conditions as during steady-state operation.

During the heating of the heat pipe, it was noticed that the evaporator end cap of the heat pipe was much brighter in color (and, thus, hotter) than the remaining portion of the heat pipe. The end cap was too close to the induction heating coils and, as a result, was being inductively heated. The portion of the heat pipe directly under the induction coils, though receiving a high-heat flux due to the inductive heating, was being cooled by the operation of the heat pipe. The end cap, however, was not cooled but was inductively coupled. The heat pipe was heated to approximately 2460°F, with a heat flux in the evaporator region (under the induction coils) of $q'' = 141$ Btu/ft^2-s and a throughput of $q = 3.1$ Btu/s. When the heat-pipe operating temperature reached ~2460°F, the temperature of the end cap of the heat pipe was approximately 2820°F. It was then noticed that the flat portion of the heat pipe had deformed outward and was no longer flat. The power to the induction heaters was turned off, and the heat pipe was allowed to cool.

After the heat pipe cooled to room temperature, it was visually inspected. The permanent deformation of the flat surface resulted in a cross-sectional thickness increase from 0.32 to 0.398 in. The increase in cross-sectional thickness was measured with a micrometer on the outside of the heat pipe. The deformation of the heat pipe occurred over nearly the entire length of the heat pipe. The last few inches of the condenser end of the heat pipe did not deform because they were at lower temperatures. In addition to the lower strength of the Mo–Re with increased temperature, the vapor pressure of the Li increases exponentially with temperature. During the initial test with the heat pipe operating at ~2370°F, the vapor pressure in the heat pipe was 11 psi, and no permanent structural deformation occurred. The vapor pressure in the heat pipe during operation at ~2460°F was $P = 16$ psi. A nonlinear finite element analysis of the Mo–Re D-shaped tube with an internal pressure of $P = 16$ psi and a temperature of $T = 2460$°F predicted a deformation of 0.014 in. vs the actual deformation of 0.08 in.

The heat pipe was next started up from the frozen state. A plot of the temperature vs time from the thermocouples is shown in Fig. 6. Thermocouple number 1 (TC 1) is in the evaporator region near the end cap, whereas TCs 2–10 are located in the condenser region. TC 4 is not shown in Fig. 6 because the data were in error. The sharp gradient at the thermal front can be observed in Fig. 6 from the sharp rise in temperature at a given location. The power to the heat pipe was increased at approximately $t = 400$ s and turned off at approximately $t = 1000$ s. Further details of this test can be found in Ref. 15.

Heat Pipes Embedded in C/C

After the design validation heat pipe was checked out and determined to operate as expected, it was decided to fabricate three additional heat pipes with the same design. After the heat pipes were fabricated and their operation verified at LANL, they were embedded in C/C and tested at NASA Langley Research Center (LaRC).

The heat-pipe containers were initially coated with an R512E oxidation protection coating. The intent was to put a coating on the heat

pipes that would protect the Mo–Re from both oxidation and carbon diffusion.[18] However, during the firing (for cleaning purposes) of the Mo–Re tubes at LANL, the coating began to evaporate. Because of the required purity for all heat-pipe fabrication steps, an attempt was made to remove the coating so that the evaporated coating would not contaminate the heat pipe during subsequent processing. Most of the coating was removed, but not all of the heat pipes appeared the same after coating removal.

Each heat pipe was wet in after it was charged with lithium. Heat pipe 1 (HP 1) was wet in for 42 h at 1650–1740°F with $m = 0.0099$ lb of Li, HP 2 was wet in for 70 h at 1650°F with $m = 0.0088$ lb of Li, and HP 3 was wet in for 47 h at 1650°F with $m = 0.018$ lb of Li. After the wet in, each heat pipe was tested to evaluate its operation.

HP 1 was heated to a uniform temperature of approximately 2300°F. Because thermocouples were not used on the heat pipes, temperatures were estimated with an optical pyrometer. With a temperature of ~2300°F and an induction heating coil length of 1.5 in., a heat flux of approximately $q'' = 155$ Btu/ft^2-s was calculated. The heat pipe was tested a second time and heated to approximately 2200°F. At this temperature, the heat pipe appeared fully isothermal with no pool at the condenser end.

HP 2 was initially operated full length at ~2420°F. It was then heated a second time. Portions of the heat pipe appeared a different color than other portions of the heat pipe due to residual R512E coating that remained on the heat pipe. The coating modified the emittance and, thus, the temperature and appearance. In the condenser section, the vapor front was not sharp but instead consisted of ~2-in.-long transition. Once the heat pipe was fully operational, it was isothermal over approximately 2 ft, with the last ~4 in. in the condenser cooler due to noncondensable gas (NCG) in the heat pipe. There was a sharp transition from the isothermal portion (~1830°F) to the cooler, NCG-filled region. The power to the heat pipe was increased until the temperature of the isothermal region was ~2075°F. At this point, the cool gas region at the condenser end was approximately 6 in. long.

HP 3 did not operate properly from the very beginning. A hot spot was observed on the flat surface of the heat pipe in the evaporator section (under the induction heating coils) from the beginning of the heating. The heat pipe was oriented such that the flat surface was facing upward. The heat pipe did operate full length at ~2330°F, but the hot spot remained during the entire test. The location of the heat source was moved toward the center of the heat pipe a few inches, but a hot spot remained under the coils during operation. The heat pipe was then wet in a second time at 1650°F for 72 h. During the next test, the heat pipe started up slightly better, but a hot spot remained under the coils. Heating was also performed in the center of the heat pipe. From the tests on HP 3, it was determined that the most likely problem with the heat pipe was a gap between the wick and the flat surface in the evaporator end. When the region with the gap was heated, a hot spot resulted because the heat was not carried away properly by a fully wetted inner surface. When the region of the heat pipe with the gap between the flat surface and the wick was not heated directly, a cool spot resulted because of poor liquid interchange between the liquid in the gap and the rest of the heat pipe.

After the heat pipes were tested, all three were embedded in C/C by Carbon–Carbon Advanced Technologies, Fort Worth, Texas. A carbon preform was previously woven by Fiberite, Greenville, Texas, with D-shaped channels using T-300 fibers. The fabric was heat treated at 3000°F. The heat treatment was not performed at as high a temperature as is often done because the use temperature of the heat-pipe test article is less than 3000°F, and higher heat treatment temperatures result in higher modulus fibers. For the application here, the lower modulus fibers resulting from the lower temperature heat treatment is preferable. A 0.005-in.-thick layer of Grafoil® was placed between the curved portion of the heat pipe and the carbon fibers prior to densification. This was done by bonding the Grafoil to the heat pipes with superglue. The purpose of the Grafoil was to serve as a compliant layer to relieve stresses due to the coefficient of thermal expansion (CTE) mismatch between the Mo–Re and the C/C. A graphite tool was used in the densification process to ensure proper positioning of the heat pipes.

A type-K thermocouple was calibrated to determine the accuracy of the thermocouples. The thermocouple was calibrated in a miniature furnace with a 392–2012°F capability. Though test temperatures were recorded above 2000°F, the calibration could be performed only to ~2000°F. An isothermal well (Inconel/steel block with holes drilled in it) was placed in the furnace. A standard National Institute of Standards and Technology (NIST) calibrated type-R thermocouple was inserted in one of the holes in the isothermal well, and the thermocouple to be calibrated was inserted in the other hole. The other ends of the thermocouples were referenced to a 32°F ice point. At each temperature set point, a stable voltage (± 1 μV) was maintained for 30 min prior to recording the voltage output. A Hewlett Packard 3457A digital multimeter was used to measure the output to within ± 1 μV. NIST ITS-90 (International Temperature Scale of 1990) thermocouple tables were used to convert the voltages to temperatures. The calibration curve comparing the standard NIST type-R thermocouple with the type-K thermocouple like those used during testing on the C/C is shown in Table 1.

The heat-pipe test article was instrumented with 34 type-K thermocouples made from the same spool of wire as the calibration thermocouple. The 24 AWG (American Wire Gage) wire thermocouples were sleeved with Nextel® ceramic sleeving. A graphite cement was used to bond the thermocouples to the C/C. The bonding surface was lightly microblasted with 2-mil-diam alumina at 80 psi to provide a matte surface for bonding. A precoat of 2–3 mils of the cement was then placed on the surface and allowed to air dry for 2 h. The entire part was then heated to 260°F in air, held for 2 h, and allowed to cool. The thermocouples were then positioned on the part and held in place with aluminum tape. The same graphite cement was then placed over the thermocouples and allowed to air dry for 2 h. The part was then heated to 260°F in air, held for 2 h, and allowed to cool. The aluminum tape was then removed, and the final step was to heat the part in air for 2 h at 450°F. Figure 7 shows a thermocouple mounted on the curved surface of the C/C. At the bottom of the figure can be seen eight thermocouple wires routed from the flat surface. Though the accuracy of the thermocouples was established from the calibration, bonding the thermocouples to the C/C introduced an unknown.

The locations of the thermocouples on the flat surface are shown in Fig. 8. The thermocouple junction was under the graphite cement, and thus its location was measured only to within $\pm\frac{1}{16}$ in. TCs 33 and 34 are on the side with the curved surface of the heat pipes (see Fig. 7) and are located opposite TCs 3 and 6, respectively. The thermocouples are positioned such that they are centered axially

Table 1 Thermocouple calibration

NIST standard thermocouple, °F	Test thermocouple, °F	Correction, °F
495.6	497.8	−2.2
997.4	1001.4	−4.0
1407.1	1411.9	−4.8
1609.2	1613.2	−4.0
1813.3	1817.4	−4.1
2019.6	2022.1	−2.5

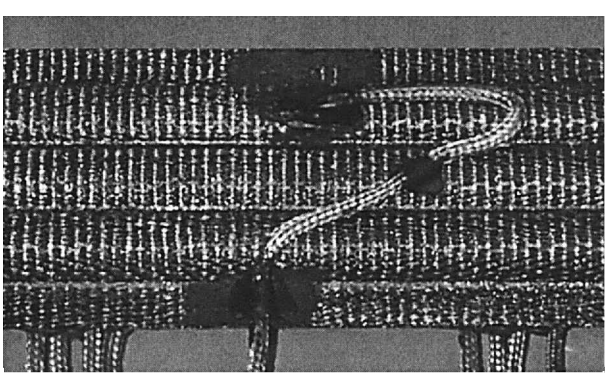

Fig. 7 Photograph of thermocouple on the curved surface of the C/C.

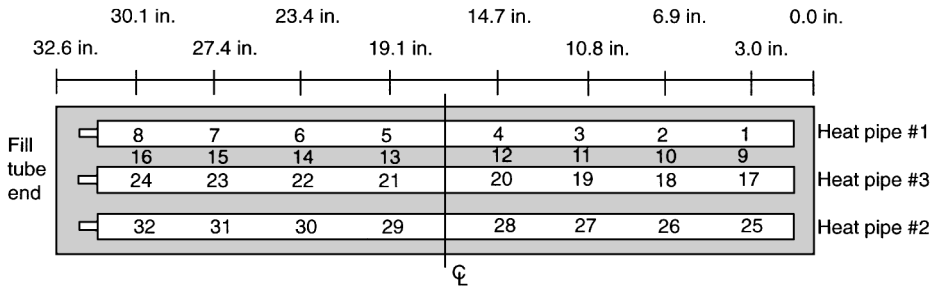

Fig. 8 Schematic drawing showing location of thermocouples on the flat surface (not to scale): $x = \pm \frac{1}{16}$ in.

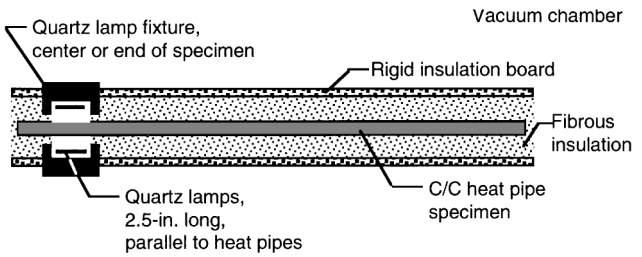

Fig. 9 Schematic drawing of test setup.

on each heat pipe (TCs 1–8 and 17–32) and in the space between two of the heat pipes (TCs 9–16). The thermocouples are located approximately 4 in. apart except at the fill tube end of the heat pipes, where the spacing is approximately 3 in.

The testing was performed in a 5-ft-diam × 5-ft-long vacuum chamber at LaRC using quartz lamps. Prior to initiation of a test, the vacuum level was usually in the $P = 10^{-6}$ torr range. During testing, the vacuum level was usually maintained in the $P = 10^{-5}$ torr range, but was in the $P = 10^{-4}$ torr range during times of significant outgassing.

A schematic drawing of the test setup is shown in Fig. 9. A total of 12 $q = \sim 0.95$ Btu/s (1 kW) quartz lamps were used, with 6 heating the upper surface and 6 heating the lower surface. The lamps, 2.5-in.-long halogen cycle lamps, were oriented parallel to the heat pipes, and thus the heated length of the heat pipes was 2.5 in. Four of the lamps were located over the sides of the heat-pipe test article (each side and both top and bottom) and, thus, did not contribute significantly to the heat flux but did help maintain a constant heat flux across the width of the test article. Fibrous insulation and rigid insulation board were used for all except the first test to insulate the test article. The insulated test article and the heating fixtures were all placed in the vacuum chamber.

Steady State

During the first test, the heat-pipe test article was completely uncovered and radiated to the inside walls of the vacuum chamber. As a result of the radiation heat losses from the test article and the limited heat input, the heat pipes never reached operating temperatures.

Because of the inability to heat the heat pipes to a level where they began to function as heat pipes, it was decided to insulate both surfaces of the heat-pipe test article outside of the heated zone. The test article was insulated with approximately 2 in. of ceramic insulation board. The insulation board was baked out for approximately 2 h at 1000°F prior to use. Fibrous Saffil® insulation (not baked out) was placed between the C/C and the rigid insulation board because the heat-pipe test article, with thermocouples and a nonflat surface, did not conform to the flat insulation board. The Saffil and insulation board were held in place with four pieces of stainless-steel wire. The heated portion of the test article was also insulated on the sides. The heat-pipe test article was insulated and positioned in the heating fixture prior to placing the entire test apparatus in the vacuum chamber. In addition to adding the insulation, the vacuum chamber was modified by placing a large (~2 × 2 ft) cold plate in the chamber for the purpose of condensing gases resulting from outgassing. The quartz lamps were centered between the thermocouples near the middle of the test article.

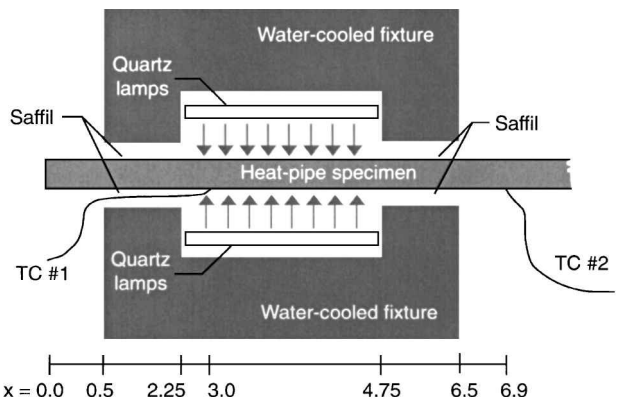

Fig. 10 Schematic drawing of the positioning (units of inches) of the thermocouples relative to the water-cooled fixture (not to scale): $x = \pm \frac{1}{16}$ in.

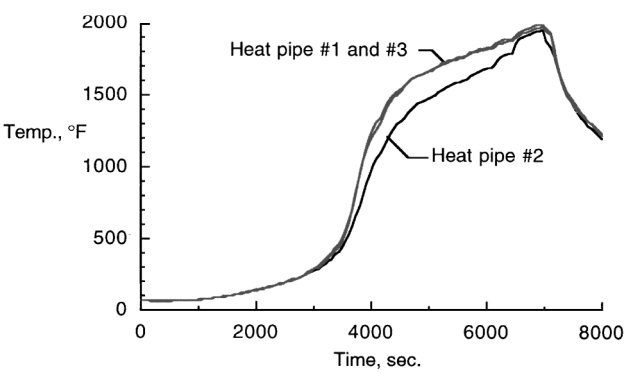

Fig. 11 Temperatures at $x = 23.3$ in. (TCs 6, 22, and 30) as a function of time for each of the three heat pipes.

The heat pipe was positioned within the heating fixture such that the heat pipe was heated at one end of the heat pipe. TC 1 ($x = 2.9$ in.) was located inside the heated region ($2.25 \leq x \leq 4.75$ in.) for TC 2 to be outside the heated region, as shown in Fig. 10. Saffil insulation was placed between the heat-pipe test article and the water-cooled fixture to reduce the heat loss radiated to the water-cooled fixture.

The heat-pipe test article was heated over a time period of approximately 2 h. Figure 11 shows the temperatures at $x = 23.3$ in. (TCs 6, 22, and 30) as a function of time. Over most of the temperature range after the heat pipes started operating, HP 2 was significantly cooler than HPs 1 and 3. However, once the higher temperatures were reached, HP 2 temperatures experienced a sudden increase to the range of the other two heat pipes.

After a few minutes at the maximum heat flux attainable with the quartz lamps, one of the quartz lamps failed, and the test was stopped. Figure 12 shows the temperatures at the maximum heat flux levels just prior to the bulb failure. The temperatures were not yet steady state, as they appeared to be slowly increasing. The temperatures of the thermocouples under the quartz lamps are also shown in Fig. 12.

Temperature distributions on the C/C over each of the three heat pipes are shown in Fig. 13 at two different heat flux levels. The

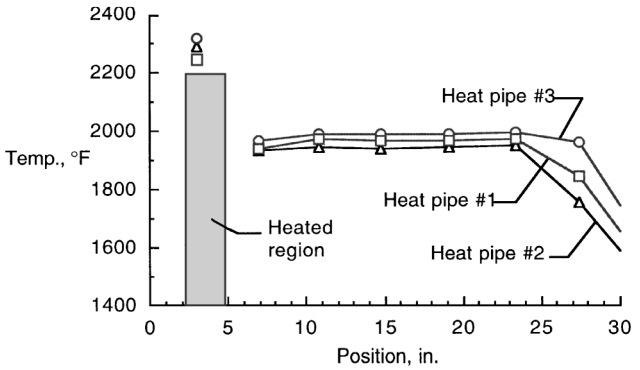

Fig. 12 Steady-state temperatures for each heat pipe in the horizontal orientation.

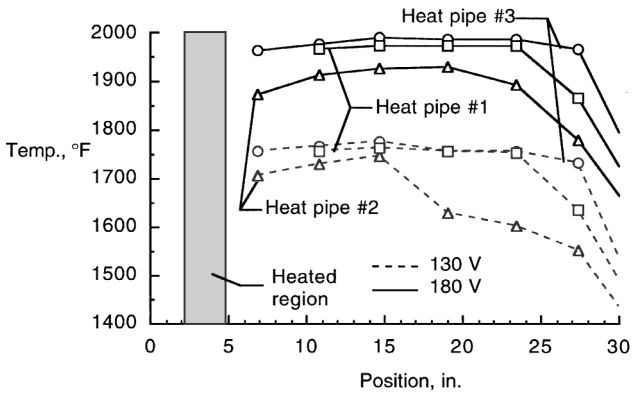

Fig. 13 Heat-pipe-temperature (on C/C) distributions in the horizontal orientation.

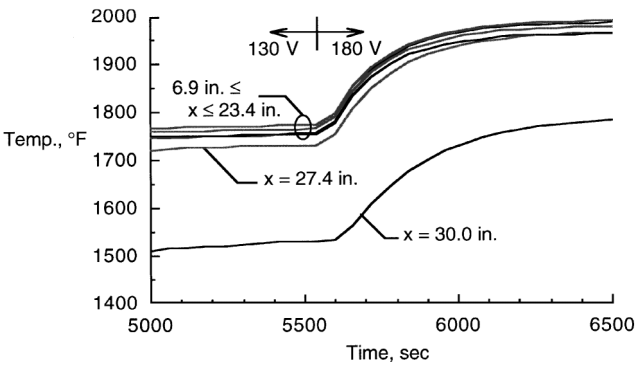

Fig. 14 Temperature distribution while transitioning from one steady-state condition to another steady-state condition in the horizontal orientation.

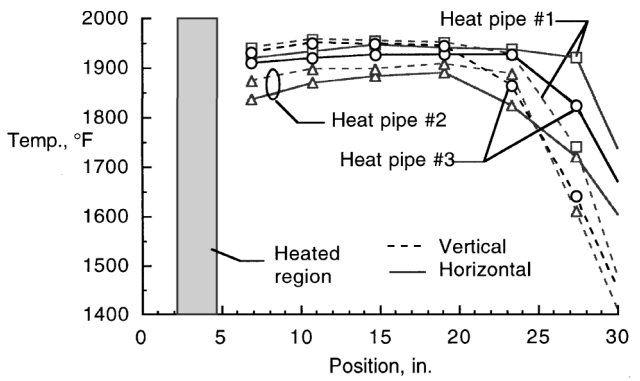

Fig. 15 Comparison of steady-state temperature distributions (180 V) over each heat pipe in both the vertical and horizontal orientations.

dashed lines represent the steady-state temperatures with a voltage of $V = 130$ V. The term steady state is used, but actually, because the test article was insulated, a true steady state was not obtained. The time required to obtain true steady-state conditions would be quite large. Steady state is used to describe the condition where only very slow increases in temperature were occurring due to the boundary effect of the insulation. The steady-state temperatures represented by the solid lines are with a voltage of $V = 180$ V. The first thermocouple outside of the heated region on HP 1 (TC 2) was not operating properly and is, thus, not shown in Fig. 13. HPs 1 and 3 were relatively isothermal over a significant length of the test article, with HP 3 isothermal over a slightly longer length. At the $V = 130$ V level, HP 2 was isothermal over a shorter length than the other two heat pipes. At the $V = 180$ V level, HP 2 temperatures were still lower than those of the other two heat pipes and appeared to have a dome-shaped distribution. The dome shape is unlike the temperature distribution shown in Fig. 12.

After a steady-state condition had been maintained at $V = 130$ V, the voltage was increased to $V = 180$ V. Figure 14 shows the transient temperature from each of the thermocouples over HP 3 prior to and after the increase in voltage. The two thermocouples farthest from the heaters at $x = 27.4$ and 30.0 in. are labeled in Fig. 14. The temperatures at the remaining locations were relatively isothermal and are not labeled. As can be seen in Fig. 14, the temperatures along the entire length of the heat pipe (even at $x = 30.0$ in.) increase together. This type of behavior is to be expected for a heat pipe. However, for heat pipes embedded in C/C, differences in thermal resistance (such as contact resistance) would result in different rise times for the temperatures at different locations. Thus, the results shown in Fig. 14 indicate that the thermal resistance between the heat pipe and the C/C was consistent along the entire length of the test article.

Though most of the testing was performed in the horizontal orientation, testing was also performed with the heat pipes vertical, heated at the top. The steady-state temperature distribution for each of the heat pipes in both the vertical and horizontal orientations is shown in Fig. 15. The voltage was 180 V in both tests. HP 2 had a dome-shaped temperature distribution, with the temperatures near the heated region lower than those near the center of the heat pipe. The temperatures of the vertical heat pipes were slightly higher than those of the horizontal heat pipes near the heated region. However, at the condenser end of the heat pipes, the vertical heat-pipe temperatures were significantly lower than the horizontal temperatures. Though the voltage to the quartz lamps was the same in both tests, a different amount of outgassing products collected on the quartz lamps reflector or slightly different insulation geometry around the heat pipes may have had an influence on the heat-pipe temperatures. In both tests, the thermocouples in the heated regions indicated similar temperatures, indicating that the heat input was not significantly different.

Startup from the Frozen State

Startup of the heat-pipe test article was performed over a time of 30 min with the heat pipes in both the vertical and horizontal orientations. The voltage to the quartz lamps was increased to 180 V in six unequal steps. The voltage was maintained at the maximum level of $V = 180$ V until a relatively steady state was obtained.

The transient temperatures over HP 1 in both orientations are shown in Fig. 16 for each of the eight thermocouples. The solid lines represent the horizontal orientation, and the dashed lines represent the vertical orientation. The first thermocouple (TC 1) was located under the quartz lamps and, thus, responded much quicker and experienced higher temperatures. Though some difference can be seen in the horizontal and vertical temperatures under the heaters (TC 1), they are similar, indicating similar heat inputs. The thermocouple next to the heated region (TC 2) did not operate properly during a portion of the horizontal test. As a result, its temperatures are shown only during the early stages of the test. The sharp increase in temperatures as the heat-pipe operating length increased down the length of the heat pipe can be seen. At steady state, the heat pipe was operating isothermally over a greater length in the horizontal orientation than in the vertical orientation. However, during the startup, the horizontal and vertical heat-pipe temperatures were similar. It was only at the higher heat fluxes and at the condenser end of the heat pipes

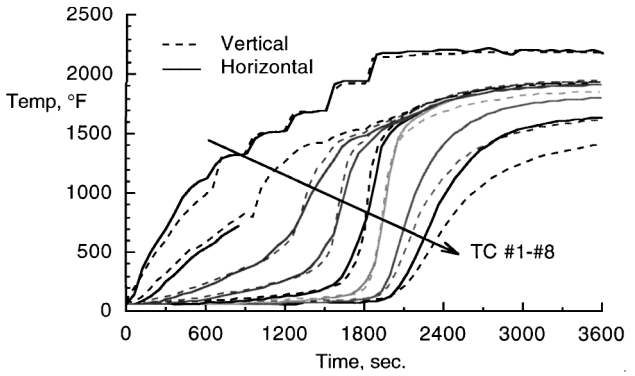

Fig. 16 Startup temperature distributions on HP 1 in the horizontal and vertical orientations.

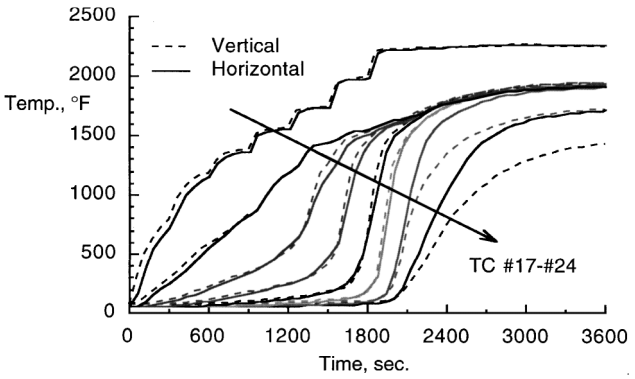

Fig. 17 Startup temperature distributions on HP 3 in the horizontal and vertical orientations.

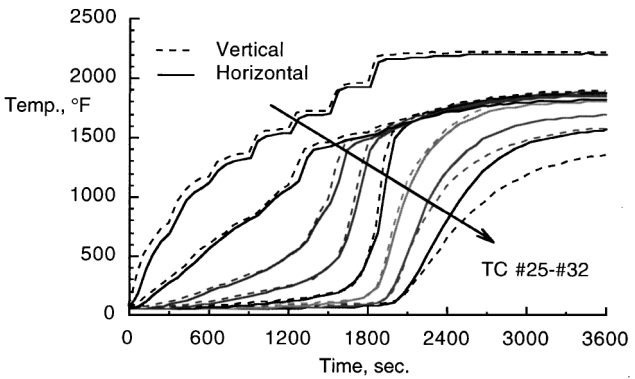

Fig. 18 Startup temperature distributions on HP 2 in the horizontal and vertical orientations.

that the vertical heat-pipe temperatures began to lag the horizontal heat-pipe temperatures. Away from the condenser end of the heat pipe, as the heat pipe was starting up, the temperature rise was steeper for the vertical heat pipe than the horizontal heat pipe. This difference can be observed by noting that the vertical heat-pipe temperature rise starts after the horizontal heat-pipe temperature rise but levels off prior to the horizontal heat-pipe temperatures.

The temperatures over HP 3, the center heat pipe in the test article, can be seen in Fig. 17 in both the horizontal and vertical orientations. The thermocouple next to the heated region (TC 2) did not operate properly during a portion of the horizontal test. As a result, its temperatures are shown only during the early stages of the test. The temperatures are similar to those in Fig. 16, except that the isothermal length was slightly larger. Figure 18 shows the temperatures over HP 2 during the startup. HPs 1 and 2 were on the sides of the test article, sandwiching HP 3 between them. That may contribute to the middle heat pipe (HP 3) being, in general, isothermal over a larger length than either of the two heat pipes on the sides.

Each of the heat pipes had a 5-mil-thick sheet of Grafoil between the heat pipe and the C/C on the curved surface of the heat pipe. On

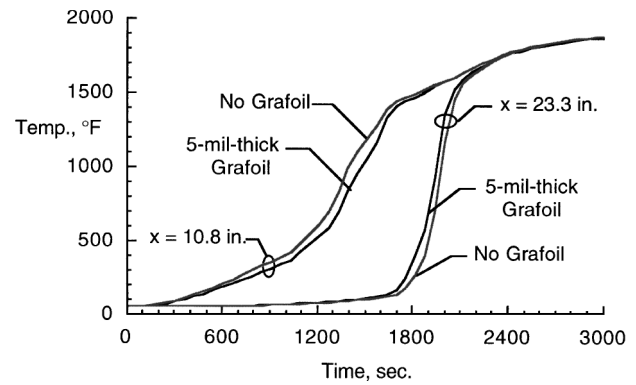

Fig. 19 Comparison of temperature rise with and without 5-mil-thick Grafoil between HP 1 and the C/C with the heat pipe in a horizontal orientation.

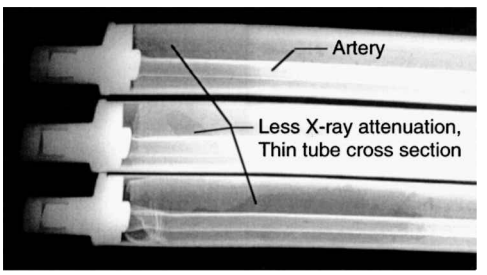

Fig. 20 X ray of the three heat pipes embedded in C/C showing the arteries in the heat pipe and areas of less attenuation.

the flat surface, which is the heated surface on an actual leading edge, no Grafoil was used in an effort to minimize the thermal resistance. Figure 19 shows the transient temperatures at $x = 10.8$ and 23.3 in. on both the flat (no Grafoil) and curved (with Grafoil) surfaces with the heat pipes in the horizontal orientation. At $x = 10.8$ in., the temperature of the surface with no Grafoil increased faster than that of the surface with Grafoil between the heat pipe and the C/C. That was as expected because the Grafoil should result in increased thermal resistance. However, at $x = 23.3$ in., the surface with no Grafoil between the C/C and the heat pipe increased slower than the surface with the Grafoil. The difference in thermal response at the two locations was also present in other horizontal tests and with the heat pipes in the vertical orientation.

Nondestructive Evaluation

Nondestructive evaluation of the C/C heat-pipe test article was performed prior to testing and after testing. Prior to testing, radiography was performed on the as-fabricated test article. Figure 20 shows an x ray of the heat pipes embedded in the C/C prior to testing. Arteries, with apparent outer diameters measured between $d = 0.135$ and 0.160 in. (design inner diameter of $d = 0.125$ in.), can be seen in each heat pipe. The difference between the artery inner and outer diameters is primarily due to the screen wick wrapped around the artery. Because of the angle of the x ray, the arteries (centered at the top, curved portion of the heat pipe) appear not to be located in the center of the heat pipes. The straight heat pipes also appear to be curved, though they are straight. The x ray revealed several areas of lower density, as indicated in Fig. 20. The lower-density areas result in less x ray attenuation and, thus, darker images. The thinner tube cross sections could be the result of the tube drawing or the sandblasting removal of the R512E coating.

Additional radiography was performed on the heat pipes after testing. The distance between the heat pipes was measured from the x rays and found to be slightly different between different heat pipes. The distance between the heat pipes varied along the length but was approximately 0.075 and 0.085 in. One gap was noticeably ($\sim$0.010 in.) wider than the other gap. The spacing was to have been 0.040 in., indicating that the gaps were approximately twice the design gap.

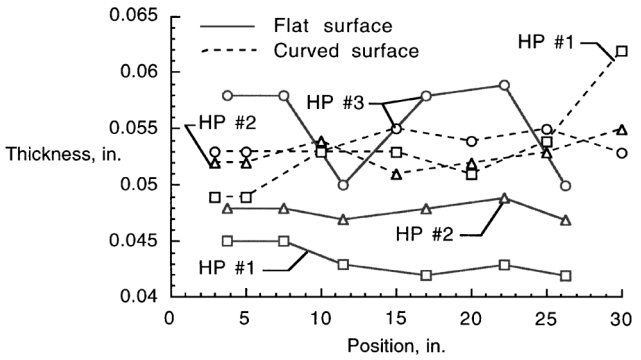

Fig. 21 Plot of thickness data (less heat-pipe container) from eddy current tests.

Eddy current liftoff thickness tests were also performed on both the flat and curved surfaces of the C/C. A 100-kHz EM6300 tester was used with an unsupported pancake probe. The data include the thickness of the C/C on the flat surface and the C/C and Grafoil on the curved surface. Any gaps would also be included in the thickness measurements. The different thicknesses may also be due to irregularities in processing or tooling. It is uncertain what the effect of the screen wick is on the thickness measurements. However, the screen is uniform over the entire length and would contribute at most 0.002–0.003 in. to the overall thickness. Figure 21 graphically shows the thicknesses along the length of each heat pipe. The thickness of the container is not included. A disbond, or gap, appears to be present on the flat surface of the center heat pipe (HP 3) at locations $x = 3\frac{3}{4}$ and $7\frac{1}{2}$ in. This hypothesis is based on both the larger thickness and the sound generated by tapping on the C/C. On the same heat pipe, at $x = 17$ and $22\frac{1}{4}$ in., the sound generated by tapping did not indicate a disbond. On the curved surface of HP 1 at $x = 30$ in., tapping on the C/C indicated a potential disbond.

During testing, HP 1 appeared to operate the best and have consistently high steady-state temperature distributions. That is consistent with Fig. 21, which indicates the thinnest C/C is over the flat surface of HP 1. However, for HPs 2 and 3, the thickness and temperatures did not always correlate. This may be because of the differences in the heat-pipe operation, i.e., presence of NCG, or because the entire test article was insulated.

Both the thickness of the C/C and the distance between heat pipes was larger in the actual test article than in the design. One technique to approach the design thickness and heat-pipe spacing is to put additional Grafoil on the curved surface between the heat pipe and the C/C. The additional Grafoil would tighten up the carbon preform because the insert (heat pipe and Grafoil) would be larger. The effect would be thinner C/C and closer-spaced heat pipes.

Concluding Remarks

The fabrication of a heat-pipe-cooled leading edge for hypersonic vehicles has moved from the preliminary design stage to the fabrication and testing of several subcomponents. The present paper discusses several heat pipes that were fabricated and tested toward this goal.

A Mo–Re D-shaped heat pipe was fabricated and successfully operated up to a temperature of 2460°F. The heat pipe was also started from the frozen state and operated as expected, verifying the design.

In addition to testing the single heat pipe, three other heat pipes were fabricated and embedded in C/C. The successful operation of each of these heat pipes was determined prior to embedding in C/C. The C/C test article with the three heat pipes was tested with quartz lamps in a vacuum chamber in both horizontal and vertical orientations. Insulation was required around the entire test article to reduce heat losses for the heat pipes to operate properly. All three heat pipes operated successfully, but each performed differently. The heat pipes were started up successfully from the frozen state numerous times. Both startup and steady-state data are presented.

The tests demonstrated that heat pipes can be embedded in C/C and successfully operated. Though the contact resistance across the interface between the heat pipe and the C/C was unknown, it was not thought to be significant based on relatively uniform surface temperatures. However, insulating the test article could also contribute to the relatively uniform temperatures. The nondestructive evaluation performed after testing indicated differences in the C/C thickness. One potential disbond area was identified, but many of the thickness variations may be due to processing or tooling irregularities.

Acknowledgments

The authors would like to thank NASA Langley Research Center for funding this work under Contract NAS1-96014. The authors would also like to thank Robert Ortega, Los Alamos National Laboratory, and Joseph G. Sikora and Jeffrey R. Knutson, NASA Langley Research Center, for their assistance in testing the heat pipes. Grafoil® is a registered trademark of Union Carbide, Nextel® is a registered trademark of 3M, and Saffil® is a trademark of Imperial Chemical Industries PLC for alumina fiber. The graphite cement used for attaching the thermocouples was a product of Dylon Industries.

References

[1]Silverstein, C. C., "A Feasibility Study of Heat-Pipe-Cooled Leading Edges for Hypersonic Cruise Aircraft," NASA CR-1857, Nov. 1971.

[2]Niblock, G. A., Reeder, J. C., and Huneidi, F., "Four Space Shuttle Wing Leading Edge Concepts," *Journal of Spacecraft and Rockets*, Vol. 11, No. 5, 1974, pp. 314–320.

[3]Alario, J. P., and Prager, R. C., "Space Shuttle Orbiter Heat Pipe Application," NASA CR-128498, April 1972.

[4]"Study of Structural Active Cooling and Heat Sink Systems for Space Shuttle," NASA CR-123912, June 1972.

[5]"Design, Fabrication, Testing, and Delivery of Shuttle Heat Pipe Leading Edge Test Modules," NASA CR-124425, April 1973.

[6]Camarda, C. J., "Analysis and Radiant Heating Tests of a Heat-Pipe-Cooled Leading Edge," NASA TN-D-8468, Aug. 1977.

[7]Camarda, C. J., "Aerothermal Tests of a Heat-Pipe-Cooled Leading Edge at Mach 7," NASA TP-1320, Nov. 1978.

[8]Camarda, C. J., and Masek, R. V., "Design, Analysis, and Tests of a Shuttle-Type Heat-Pipe-Cooled Leading Edge," *Journal of Spacecraft and Rockets*, Vol. 18, No. 1, 1981, pp. 71–78.

[9]Peeples, M. E., Reeder, J. C., and Sontag, K. E., "Thermostructural Applications of Heat Pipes," NASA CR-159096, June 1979.

[10]Boman, B. L., Citrin, E. C., Garner, E. C., and Stone, J. E., "Heat Pipes for Wing Leading Edges of Hypersonic Vehicles," NASA CR-181922, Jan. 1990.

[11]Boman, B. L., and Elias, T., "Tests on a Sodium/Hastelloy X Wing Leading Edge Heat Pipe for Hypersonic Vehicles," AIAA Paper 90-1759, June 1990.

[12]Colwell, G. T., Jang, J. H., and Camarda, C. J., "Modeling of Startup from the Frozen State," 6th International Heat Pipe Conf., Grenoble, France, May 1987.

[13]Glass, D. E., and Camarda, C. J., "Preliminary Thermal/Structural Analysis of a Carbon–Carbon/Refractory-Metal Heat-Pipe-Cooled Wing Leading Edge," *Thermal Structures and Materials for High Speed Flight*, edited by E. A. Thornton, Vol. 140, Progress in Astronautics and Aeronautics, AIAA, Washington, DC, 1992, pp. 301–322.

[14]Rovang, R. D., Palamides, T. R., and Hunt, M. E., "Fabrication of Carbon-Carbon Heat Pipes for Space Nuclear Power Applications," 27th Intersociety Energy Conversion Engineering Conf., San Diego, CA, Aug. 1992.

[15]Glass, D. E., Merrigan, M. A., and Sena, J. T., "Fabrication and Testing of Mo-Re Heat Pipes Embedded in Carbon/Carbon," NASA CR-1998-207642, March 1998.

[16]Glass, D. E., Camarda, C. J., and Merrigan, M. A., "Refractory-Composite/Heat-Pipe-Cooled Leading Edge," U.S. Patent 5,720,339, Feb. 1998.

[17]Merrigan, M. A., Keddy, E. S., and Sena, J. T., "Transient Performance Investigation of a Space Power System Heat Pipe," AIAA Paper 86-1273, June 1986.

[18]Glass, D. E., "Oxidation and Emittance Studies of Coated Mo-Re," NASA CR-201753, Oct. 1997.

H. L. McManus
Associate Editor